CEAI, Vol.23, No.4, pp. 86-94, 2021 Printed in Romania

Nonlinear Model Predictive Speed Control with Variable Predictive Horizon for PMSM Rotor Position

**Yao Wei, Yanjun Wei*, Shuo Yuan, Hanhong Qi*,
Xiaoqiang Guo, Mengyuan Li**

*College of Electrical Engineering, Yanshan University, Qinhuangdao 066004 China
(Tel: 86-335-8058471, e-mail: weiyao@stumail.ysu.edu.cn, yjwei@ysu.edu.cn*,18856319368@163.com, hhqi@ysu.edu.cn*, yedumin@163.com, l253424371@outlook.com).*

Abstract: Predictive horizon in model predictive control (MPC) or nonlinear MPC (NMPC) is a constant value which limits the performance of system. A nonlinear model predictive speed control (NMPSC) with variable predictive horizon during each sampling period is proposed in this paper, and applied into the rotor position control system of permanent magnet synchronous motor (PMSM). The prediction horizon can be adjusted to improve control accuracy and decrease calculation burden. The proposed method is compared with the improved NMPSC strategy with extra weighting factors, and it exhibits high performances in tracking process, robustness of stator resistance and magnet flux linkage mismatches. Even with rated load torque, the proposed method still achieves high servo stiffness. Simulation and experimental results verify the effectiveness and feasibility of the proposed control strategy, under the condition of a sinusoidal reference which makes system operate in transient state continuously.

Keywords: NMPSC, PMSM, Predictive horizon, Parameter mismatches.

1. INTRODUCTION

Permanent magnet synchronous motor (PMSM) is a frequently used device in industry that requires high power density, efficiency and torque-ampere ratio with light weight and volume such as robotic manipulator. Moreover, the control strategies for power converters and motor drives having been constantly developed with the performances of the control algorithms, digital processors, semiconductor devices and planted topologies (Wang et al., 2019; Mubarok et al., 2019). MPC strategy has been highlighted and generated during recent years because of high dynamics and easy understanding, and has been wildly applied in power electronic realm (Rodriguez et al., 2012; Nguyen et al., 2018; Zhang et al., 2017).

MPC can be divided as continuous control set-MPC (CCS-MPC) and finite control set-MPC (FCS-MPC) (Rodriguez et al., 2012). With a modulation module, prediction horizon of CCS-MPC covers hundreds of sampling periods, and has less ripple and switching losses comparing with the FCS-MPC. But the prediction horizon cannot be adjusted as convenient as FCS-MPC to improve control performances (Wei et al., 2020). Conventional FCS-MPC belongs to short prediction horizon method which only covers single sampling period. In the digital system, delays in calculation and transmission processes may affect the predictive performances (Norambuena et al., 2019). In order to enhance the stability and the tracking performance, the prediction horizon should be prolonged to cover more sampling periods to compensate the delays. Based on this idea, some methods such as the sequential MPC (SMPC), parallel MPC (PMPC) and nonlinear MPC (NMPC) are proposed with prolonged prediction horizon (Wang, 2014; Geyer, 2016).

SMPC and PMPC are proposed to eliminate the weighting factors. The predictive variables are prolonged at time k+2 in both methods according to the one-step delay compensation method, and it belongs to the long prediction horizon method (Cortes et al., 2012). In PMPC, a switching vectors intersection method is inserted into a model predictive torque control (MPTC) structure to select an optimal vector to obtain better robustness and dynamics (Wang et al., 2020). In SMPC, the cost function in the conventional MPC is split into multiple cost functions with single objective or variable, and an optimal vector is selected by sifting according to the control objectives repeatedly (Zhang et al., 2016; Wang et al., 2017). SMPC can be combined with a cascade MPC (CMPC) strategy to realize a kind of composite structure to achieve different objectives effectively (Andrés et al., 2019). The number of control objectives is strictly restricted due to the limited voltage vectors of the switching table. A possibility of more control objectives can be presented by a group of extra-vectors and topologies with extra-switches (Wu et al., 2019).

The prediction horizons of SMPC and PMPC can only cover two sampling periods by the one-step delay compensation method. NMPC has an accumulating nonlinear cost function which includes the control objectives with different sampling periods (Xiao et al., 2019), and has been used in many applications in model driving and power electronic realms to realize long predictive horizon, especially in electrical control system with high performance for electrical vehicle (Vera et al., 2019; Chen et al., 2020; Tavernini et al., 2019; Vafamand, et al., 2019). A serial of weighting factors converging to zero are inserted to the cost function to enhance the convergence speed and stability of the system (Younesi et al., 2018; Younesi et al., 2018). An adaptive dynamic programming (ADP) algorithm is combined with the NMPC strategy to further improve the robustness and dynamics (Dong et al., 2019).

MPC on the PMSM system can be mainly divided into model predictive current control (MPCC), model predictive speed control (MPSC) and MPTC according to the primary controlled objective, and can be extended to the NMPC strategy such as nonlinear MPSC (NMPSC) strategy (Zhang, et al., 2020; Yan et al., 2020; Gao et al., 2020). Although better stability and rapidity in NMPC can be accomplished by the prolonged prediction horizon, the calculation burden and prediction error are increased sharply at the same time. As a result, the prediction horizon needs to be adjusted according to the control objectives and operating states. A variable predictive horizon is inserted to the NMPC to tune the predictive horizon. A NMPSC with a variable repetitive number of the predictive processes according to the angular velocity error is proposed for PMSM rotor position tracking system in this paper, the predictive horizon is a variable and tuned at each sampling periods by the varied repetitive number. Prediction errors caused by the interpolation method and parameter mismatches are analysed with different predictive horizons in detail. The correctness and advantages including robustness of stator resistance and magnet flux linkage, servo stiffness and tracking performance are verified by the simulation and experimental results.

2. PREDICTION ERROR ANALYSIS FOR NMPSC

2.1 PMSM Discrete-time Model

Based on the two phase synchronized rotation reference frame, the state functions of the model of PMSM can be expressed as follows. The continuous-time model functions including the stator voltage u_s, flux linkage ψ_m, electromagnetic torque T_e and the angular velocity ω_r are expressed as:

$$\begin{cases} u_{sd} = R_s i_{sd} + L_s \dfrac{di_{sd}}{dt} - L_s \omega_r i_{sq} \\ u_{sq} = R_s i_{sq} + L_s \dfrac{di_{sq}}{dt} + L_s \omega_r i_{sd} + j\psi_m \omega_r \end{cases} \tag{1}$$

$$\begin{cases} \psi_{sd} = L_s i_{sd} + \psi_m \\ \psi_{sq} = L_s i_{sq} \end{cases} \tag{2}$$

$$T_e = \frac{3}{2} p \psi_m i_{sq} \tag{3}$$

$$\frac{d\omega_r}{dt} = \frac{p}{J}\left(T_e - T_L\right) - \frac{B}{J}\omega_r \tag{4}$$

where subscripts d and q mean that the vari ables locate at the d-axis or q-axis respectively. Moreover, L_s is the stator self-inductance, R_s is the stator resistance, p is the number of pole pairs, J is the rotor inertia, B is the friction coefficient and the ψ_m is the flux magnitude due to the rotor magnets.

Based on sampling time T_s, two-step Euler interpolation method including predicting step $\boldsymbol{x}_p(k+1)$ and correcting step $\boldsymbol{x}(k+1)$ is adopted to predict and discrete the model, and the discrete model can be obtained as:

$$\begin{cases} \boldsymbol{x}_p(k+1) = \boldsymbol{x}(k) + T_s h\left(\boldsymbol{x}(k), \boldsymbol{u}(k)\right) \\ \boldsymbol{x}(k+1) = \boldsymbol{x}(k) + \dfrac{T_s}{2}\left(h\left(\boldsymbol{x}(k), \boldsymbol{u}(k)\right) + h\left(\boldsymbol{x}_p(k+1), \boldsymbol{u}(k)\right)\right) \end{cases} \tag{5}$$

where

$$\boldsymbol{x}(k) = \begin{bmatrix} i_{sd}(k) & i_{sq}(k) & \omega_r(k) \end{bmatrix} \tag{6}$$

$$\boldsymbol{u}(k) = \begin{bmatrix} u_{sd}(k) & u_{sq}(k) \end{bmatrix} \tag{7}$$

$$h\left(\boldsymbol{x}(k), \boldsymbol{u}(k)\right) = \begin{bmatrix} -\dfrac{R_s}{L_s} i_{sd}(k) + \omega_r(k) i_{sq}(k) + \dfrac{1}{L_s} u_{sd}(k) \\ -\dfrac{R_s}{L_s} i_{sq}(k) - \omega_r(k) i_{sd}(k) - \dfrac{\psi_m}{L_s}\omega_r(k) + \dfrac{1}{L_s} u_{sq}(k) \\ \dfrac{3p^2\psi_m}{2J} i_{sq}(k) - \dfrac{B}{J}\omega_r(k) \end{bmatrix} \tag{8}$$

2.2 Conventional Control Strategy

The control objectives of PMSM system are speed reference tracking and ampere optimized torque, than the cost function can be expressed as:

$$J = \sum_{j=1}^{P}\left[\lambda_\omega\left(\omega_r^* - \omega_r(k+j)\right)^2 + \lambda_i i_{sd}^2(k+j)\right] \tag{9}$$

where λ_ω and λ_i are weighting factors, P is repetitive number of predictive processes, and the prediction horizon equals to $P*T_s$. The first term of (9) evaluates the minimal predictive speed error between actual speed ω_r and reference speed ω_r^*, and the second term minimizes i_{sd} for optimized torque by ampere ratio which is same as $i_{sd}^* = 0$ method in conventional vector control of PMSM.

The operation of the NMPSC with $P = 4$ with delay and long calculation time is shown in Fig. 1, where $\omega_{r|k+1}$ is the actual angular velocity at time k+1. At time k+4, for different vectors, ω_r may have several predictive values $\omega_r(k+4)$ as shown in the figure. The selected vector at time k+4 may not be the optimal vector at time k+1 such as the blue line in the figure, and the system maybe unstable. Comparing with the one-step delay compensation method in (Rodriguez et al., 2012) and (Cortes et al., 2012), the NMPSC might have possibility of instable operation in compensating delay and controlling system.

An improved cost function of NMPSC is:

$$J = \sum_{j=1}^{P} Q_j \left[\lambda_\omega\left(\omega_r^* - \omega_r(k+j)\right)^2 + \lambda_i i_{sd}^2(k+j)\right] \tag{10}$$

where Q_j is a group of weighting factors to distinguish the importance of control objectives with different prediction horizons and to improve convergence of the system. An effective tuning method of Q_j is:

$$Q_j = \frac{1}{1+j} \tag{11}$$

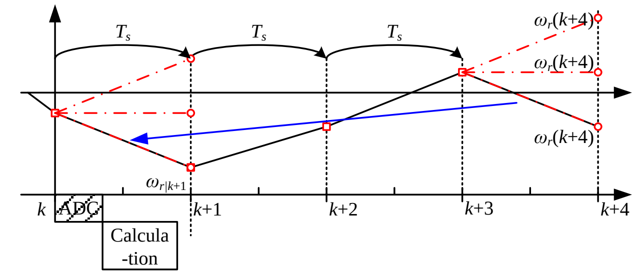

Fig. 1. Operation of the NMPSC with delay and long calculation time.

A longer prediction horizon makes the system operate in transient state stably and quickly, taking more than one sampling periods into consideration. These predictive variables at time $k+j$ (j > 1) have fewer effects to the final value of cost function comparing with the predictive variables at time k+1 to ensure stability and convergence.

3. NMPSC WITH VARIABLE PREDICTIVE HORIZON

3.1 Control Strategy

The repetitive number of predictive processes P is changed as a positive integral discrete-time variable P_{k+1} which is adjusted during each sampling periods, and the cost function (10) is advanced as:

$$J = \sum_{j=1}^{P_{k+1}} Q_j \left[\lambda_\omega \left(\omega_r^* - \omega_r \left(k+j \right) \right)^2 + \lambda_i i_{sd}^2 \left(k+j \right) \right] \tag{12}$$

and P_{k+1} is satisfying:

$$P_{k+1} = \begin{cases} P_M & if \quad P_{k+1} > P_M \\ P_k + \operatorname{sgn}\left(e_{k+1} - e_k \right) \cdot \Delta P & if \quad P_M \geq P_{k+1} \geq 1 \\ 1 & if \quad P_{k+1} < 1 \end{cases} \tag{13}$$

where P_M is the maximal threshold and ΔP is the changing step of the repetitive number satisfying $\Delta P \in \square^{+}$. e_k is the error of the angular velocity ω_r at time k, and the function sgn() is a sign function which can be expressed as:

$$\operatorname{sgn}\left(e_k - e_{k-1} \right) = \begin{cases} 1 & if \quad e_k - e_{k-1} > 0 \\ 0 & if \quad e_k - e_{k-1} = 0 \\ -1 & if \quad e_k - e_{k-1} < 0 \end{cases} \tag{14}$$

and the prediction horizon at time k+1 is also a discrete-time variable equalling $P_{k+1} * T_s$.

The structure of the NMPSC with variable repetitive number is shown in Fig. 2. When the error at time k+1 is larger than time k, the repetitive number P is increased to prolong the prediction horizon and to make the system operate in transient processes more stably. Similarly, the repetitive number P is decreased to reduce hardware calculation burden when the error at time k+1 is less than time k.

3.2 Prediction Error for the Proposed NMPSC

3.2.1 Interpolation Method Accuracy

The two-step Euler interpolation method has been used repeatedly to realize long prediction horizon. During a sampling period, the prediction error at $k+P$-th sampling period is:

$$\omega_{r|k+P} - \omega_r \left(k+P \right) \approx -\frac{T_s^3}{12} \omega_{r|k+P-1} \tag{15}$$

When the repetitive number of predictive processes is growing up, the prediction errors are increasing because:

$$\left| \frac{\omega_{r|k+P} - \omega_r \left(k+P \right)}{\omega_{r|k+P-1} - \omega_r \left(k+P-1 \right)} \right| \approx \left| \frac{-\dfrac{T_s^3}{12} \omega_{r|k+P-1}}{\omega_{r|k+P-1} - \omega_r \left(k+P-1 \right)} \right| \tag{16}$$

$$< \left| \frac{\omega_{r|k+P-1}}{\omega_{r|k+P-1} - \omega_r \left(k+P-1 \right)} \right| < 1$$

i. e.:

$$\left| \omega_{r|k+P} - \omega_r \left(k+P \right) \right| < \left| \omega_{r|k+P-1} - \omega_r \left(k+P-1 \right) \right| \tag{17}$$

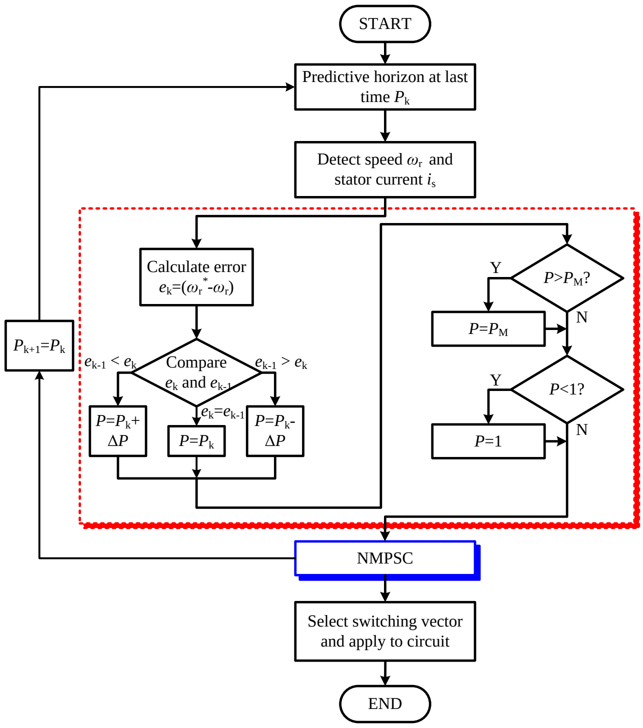

Fig. 2. Flowchart of the NMPSC with variable predictive horizon.

When the repetitive number P equals to P_M, the maximum value of prediction error E_{i1} of the NMPSC can be expressed as follow. The prediction error is accumulated due to the repetitive predictive processes, and it is converged to a constant value if the prediction horizon tends to infinity.

$$E_{i1} = \sum_{i=1}^{P_M} \left| \omega_{r|k+i} - \omega_r \left(k+i \right) \right| \tag{18}$$

Similarly, the predictive error E_{i2} of the improving NMPSC is equalled to E_{i1}, and the prediction error E_{i3} for the NMPSC with the variable repetitive number P_{k+1} can be expressed as:

$$E_{i3} = \sum_{i=1}^{P_{k+1}} \left| \omega_{r|k+i} - \omega_r\left(k+i\right) \right| \tag{19}$$

The prediction error is accumulated with the increasing of repetitive number of predictive processes. Comparing with (18) and (19), the prediction error caused by the interpolation method can be reduced by changing the repetitive number and prediction horizon when the system does not need a large repetitive number.

3.2.2 Parameter Sensitivities

The two-step Euler interpolation method at time $k+P$ can be expressed as:

$$\begin{aligned} \omega_r\left(k+P\right) &= \omega_r\left(k+P-1\right) + \frac{T_s}{2}\left[\frac{3p^2\psi_m}{2J} i_{sq}\left(k+P-1\right)\right. \\ &\left. -\frac{B}{J}\omega_r\left(k+P-1\right) + \frac{3p^2\psi_m}{2J}\hat{i}_{sq}\left(k+P\right) - \frac{B}{J}\hat{\omega}_r\left(k+P\right)\right] \end{aligned} \tag{20}$$

and the predictive step variables are:

$$\begin{aligned} \hat{\omega}_r\left(k+P\right) &= \omega_r\left(k+P-1\right) \\ &+T_s\left[\frac{3p^2\psi_m}{2J} i_{sq}\left(k+P-1\right) - \frac{B}{J}\omega_r\left(k+P-1\right)\right] \end{aligned} \tag{21}$$

$$\begin{aligned} \hat{i}_{sq}\left(k+P\right) &= i_{sq}\left(k+P-1\right) + T_s\left[-\frac{R_s}{L_s} i_{sq}\left(k+P-1\right)\right. \\ &\left. -\omega_r\left(k+P-1\right) i_{sd}\left(k+P-1\right) - \frac{\psi_m}{L_s}\omega_r\left(k+P-1\right) - \frac{1}{L_s}u_{sq}\left(k\right)\right] \end{aligned} \tag{22}$$

The angle velocity prediction error due to model parameter mismatches in stator resistance R_s, stator induction L_s and magnet flux linkage ψ_m are inevitable (Yan et al., 2020; Siami et al., 2017). Defining the model parameters with mismatches as R_{se}, L_{se} and ψ_{me} respectively, the variation trends of prediction errors with different R_{se}/R_s, L_{se}/L_s and ψ_{me}/ψ_m are shown in Fig. 3.

Under R_{se} with negative mismatch conditions (i. e. $R_{se}/R_s < 1$), the prediction errors decrease to zero when the parameter has no mismatch, and then under R_{se} with positive mismatch conditions (i. e. $R_{se}/R_s > 1$), the prediction errors increase from zero with the growing of R_{se}/R_s. The prediction error is the lowest when the repetitive number P equals to 2, and it is the highest when the repetitive number P equals to 5.

The prediction error waveforms with different stator induction mismatches and repetitive numbers show that under the negative mismatch conditions (i. e. $L_{se}/L_s < 1$) the prediction errors decrease, and arrive to zero when the parameter has no mismatch. Under the positive mismatch conditions (i. e. $L_{se}/L_s > 1$), they increase from zero to some constant values. These constant values and the prediction errors increase with the increasing of repetitive numbers.

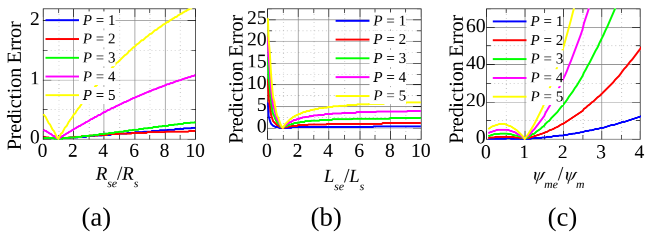

Fig. 3. Prediction error waveforms with different predictive horizons and parameter mismatches. (a) Stator resistance, (b) Stator induction, (c) Magnet flux linkage.

For different magnet flux linkage mismatches, the figure shows that under the conditions of negative mismatches (i. e. $\psi_{me}/\psi_m < 1$), the prediction errors increase at first and decrease to zero when the parameter has no mismatch, and then increase sharply from zero to infinity under the conditions of positive mismatches (i. e. $\psi_{me}/\psi_m > 1$). The relationships between prediction errors and repetitive numbers are similar for the stator induction and magnet flux linkage mismatches, larger repetitive number will bring higher prediction error.

The influences of R_{se}, L_{se} and ψ_{me} on speed prediction at PMSM's rated state are analysed in Fig. 4 under the condition of the repetitive number as 5. The prediction errors increase with the growing of R_{se}/R_s under the stator induction positive mismatches condition, and under other conditions, the prediction errors decrease to zero and then begin to increase as shown in Fig. 4(a). The locations of zero prediction errors are different under multi-parameter mismatches. In Fig. 4(b), the prediction errors from stator resistance and magnet flux linkage mismatches decrease with different slopes by the increasing of R_{se}/R_s, except that it increase under the condition of no mismatch.

The prediction errors with stator resistance and stator induction mismatches decrease to zero near the no mismatch point of L_{se}/L_s, and then increase from zero to similar values as shown in Fig. 4(c). In Fig. 4(d), the prediction errors with magnet flux linkage and stator induction mismatches decrease to zero at first, and then increase from zero to similar values. Fewer mismatches lead the prediction error to reach to zero earlier.

The prediction errors under the condition of mismatches of the stator resistance and magnet flux linkage are shown in Fig. 4(e). The prediction errors increase to about 8 at first and decrease to zero near the no mismatch point of the magnet flux linkage, and then increase sharply with the increasing of ψ_{me}/ψ_m. The prediction errors under the stator induction and magnet flux linkage mismatches conditions are shown in Fig. 4(f), it has the similar trend with Fig. 4(e), but it's more dispersed.

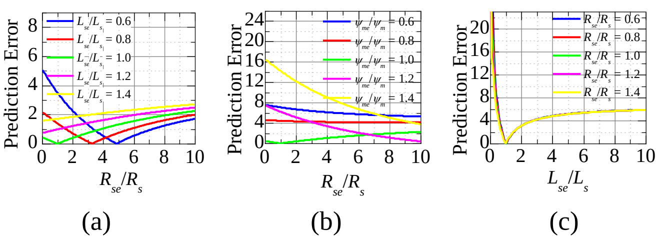

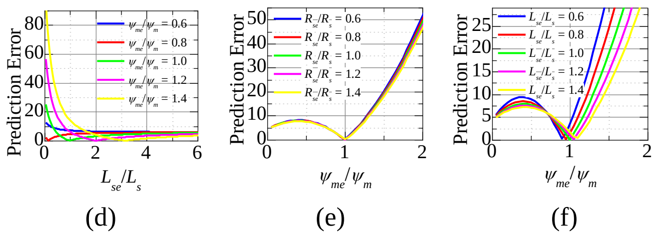

Fig. 4. Prediction error waveforms with different parameter mismatches. (a) Stator resistance and induction mismatches, (b) Stator resistance and magnet flux linkage mismatches, (c) Stator induction and resistance mismatches. (d) Stator induction and magnet flux linkage mismatches, (e) Magnet flux linkage and stator resistance mismatches, (f) Magnet flux linkage and stator induction mismatches.

The above three kinds of parameter mismatches can all lead to prediction error, the heavier the mismatch the larger the prediction error, and the stator induction has the greatest influence on the prediction error.

4. SIMULATION RESULTS

The simulation study is carried out on the simulink toolbox of the MATLAB software. The model structure is shown in Fig. 5 and the main parameters are listed in Tab. I respectively. A proportional controller has been selected as the rotor position controller because of the rapidity, which is the main objective of the rotor position control system (Wei et al., 2020; Kou et al., 2008).

4.1 Tracking Performance

A sinusoidal wave with amplitude 10 rad, frequency 5Hz and zero initial phases is selected as the rotor position reference signal θ^* to test the tracking performance of the system. The waveforms of θ, θ^* and their errors are shown in Fig. 6. The figure shows that the rotor position θ can track the sinusoidal reference successfully with the maximal delay time about 4 ms and ITAE 0.2552 in 0.8s. The rotor position error has the maximal value because the maximal delay times happen at the crossing zero points.

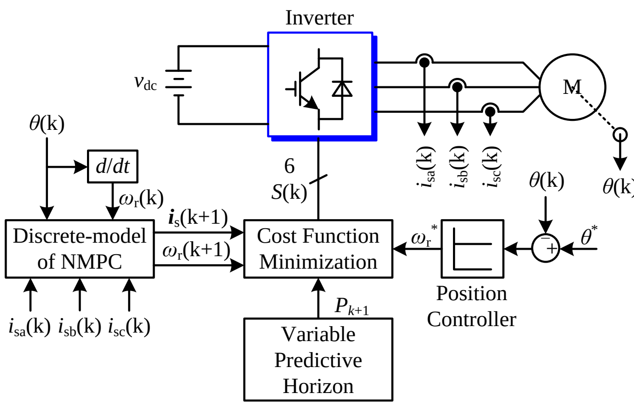

Fig. 5. Structure of NMPSC with variable predictive horizon.

Comparing with the improved NMPSC strategy in (10) with repetitive numbers from 1 to 29 after seven accumulating steps as shown in Fig. 7, the rotor position error increases with the growing of the repetitive number, and result in the distortion of rotor position. The proposed method prolongs the repetitive number of the predictive processes of NMPSC and ensures the stability during several sampling periods.

Table 1. Simulation main parameters.

Symbol	Quantity	Value
R_s	Stator resistance	2.875Ω
L_s	Stator self-inductance	0.835mH
J	Rotor inertia	0.0008kg.m^2
B	Friction coefficient	0.0008N.m.s
p	The number of pole pairs	4
ψ_m	Flux magnitude due to the rotor magnets	0.175Wb
T_s	Sampling time	25μs
P_M	Repetitive number maximal threshold	150 (3 in experiments)
P_r	Rotor position proportional controller parameter	120
n_n	Rate speed	3000rpm
f_n	Rate frequency	200Hz
P_n	Rate power	1kW
I_n	Rate current	3.65A
v_{dc}	Voltage of DC source	700V

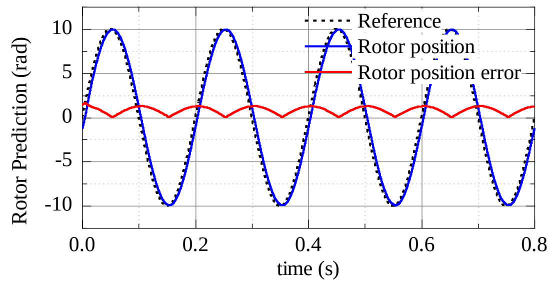

Fig. 6. Tracking performance for the proposed method in simulation.

4.2 Robustness Analysis

Simulations of the proposed strategy and the improved strategy with repetitive number 5 are performed for comparison, under the conditions of stator resistance mismatches, stator induction mismatches and magnet flux linkage mismatches respectively. For the stator resistance mismatches, the simulation results of rotor position and its error as shown in Fig. 8, the system can operate stably within the whole testing range for the proposed method, but the stable upper bound of R_{se}/R_s for the improved NMPSC strategy is restricted to about 75.

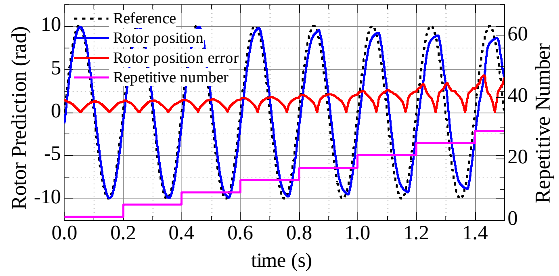

Fig. 7. Tracking performance for the improved NMPSC with the increasing repetitive numbers.

For the stator induction mismatches, the simulation results are shown in Fig.9. Comparing with the improved method with a stable range about 0.5~∞, but for the proposed method, it is about 0.2~200. The lower bound is expended and the upper bound is reduced.

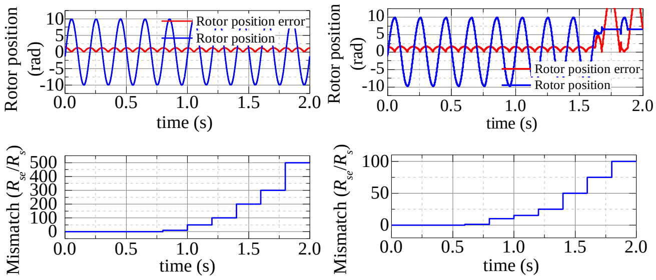

(a) (b)

Fig. 8. Rotor position and its errors with different stator resistance mismatch values. (a) Proposed strategy, (b) Improved strategy.

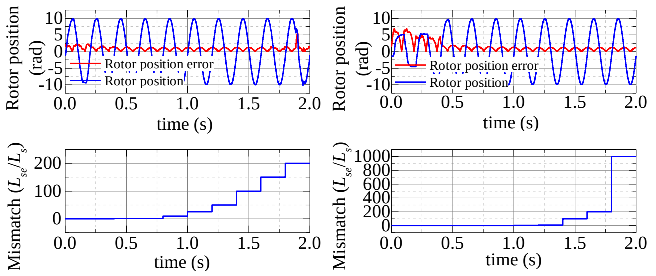

(a) (b)

Fig. 9. Rotor position and its errors with different stator induction mismatch values. (a) Proposed strategy, (b) Improved strategy.

For the magnet flux linkage mismatches, the simulation results of rotor position and its error are shown in Fig. 10, The stable range for the proposed method is about 0.1~20, and it is about 1~10.

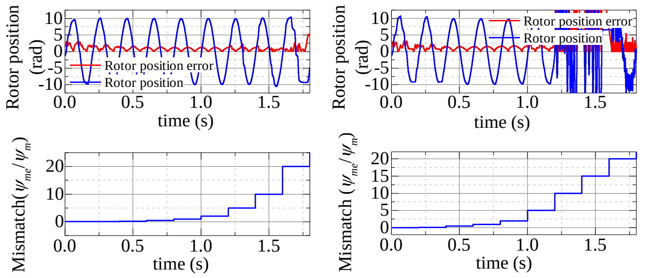

(a) (b)

Fig. 10. Rotor position and its errors with different magnet flux linkage mismatch values. (a) Proposed strategy, (b) Improved strategy.

The robustness for the proposed method and the improved method are listed in Tab. II, which shows that the robustness under the condition of the stator resistance and magnet flux linkage mismatches are improved for the proposed strategy. The stable ranges of the stator resistance and magnet flux linkage mismatches for the proposed strategy are increased about 85.0% and 54.77% respectively, but the stator induction mismatch range is decreased about 80.01%.

Table 2. Robustness analysis.

Control method	Stator resistance mismatch	Stator induction mismatch	Magnet flux linkage mismatch
Proposed NMPSC with variable repetitive number	-	0.2~200	0.1~20
Improved NMPSC	~75	0.5~∞	1~10

4.3 *Weighting Factor Sensitivities*

The weighting factors λ_ω and λ_i are designed to distinguish the importances. A typical selecting method is the branch and bound algorithm which is based on a lot of simulations and experiments (Rodriguez et al., 2012). The rotor position ITAEs with different weighting factor values are shown in Fig. 11. It can be seen that the ITAEs decrease with the increasing of λ_ω and decreasing of λ_i. Under different weighting factors, the maximal speed error, maximal acceleration and maximal predictive horizon are shown in Fig. 12, and they decrease with the increasing λ_ω of and decreasing of λ_i. According to the simulation results above, the weighting factors λ_ω and λ_i are selected as 1.0 and 0.2 respectively to ensure suitable performances.

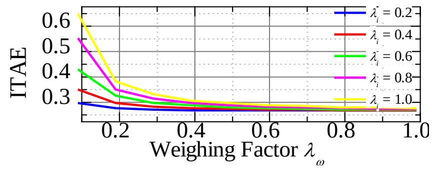

(a)

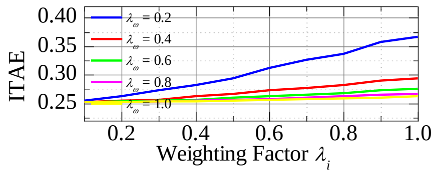

(b)

Fig. 11. Rotor position ITAEs with different weighting factors. (a) weighting factor λω, (b) weighting factor λi.

4.4 *Servo Stiffness Analysis*

The servo stiffness is an important performance for the rotor position control system, which reflects the rotating angle $\Delta\theta$ of a zero rotor position reference with a load torque T_L, and the definition of servo stiffness K can be expressed as:

$$K = \left|\Delta\theta / T_L\right| \tag{23}$$

The simulation results of the servo stiffness K for the proposed strategy (with blue line) and the improved strategy with different P (3 in red, 5 in green and 7 in pink) are shown in Fig. 13, and the average values and standard deviation values of servo stiffness K for four operating states are listed in Tab. III.

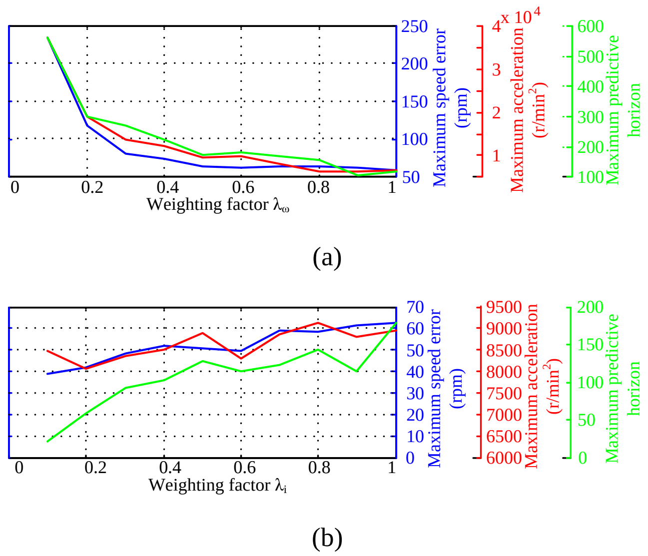

Fig. 12. Different performance indexes with different weighting factors. (a) weighting factor λω, (b) weighting factor λi.

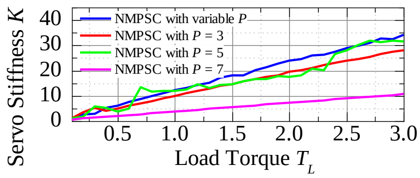

Fig. 13. Servo stiffness with different repetitive number.

As shown in the figure and the table, the proposed method has larger average servo stiffness and standard deviation comparing with the improved NMPSC. And for the improved NMPSC, the servo stiffness has minimal values with the repetitive number of 7. The repetitive number P can be adjust automatically for the proposed method to obtain a suitable servo stiffness.

Table 3. Servo stiffness analysis.

Control method	Repetitive number	Average value of servo stiffness	Standard deviation value of servo stiffness
Proposed NMPSC with variable repetitive number P	Variable	18.164	9.951
Improved NMPSC	3	15.114	8.079
	5	16.528	9.259
	7	5.713	3.056

5. EXPERIMENTAL RESULTS

The setup is shown in Fig. 14, and a three-phase inverter with IGBTs (FGL35N120FTD) and a 1kW PMSM (INOVANCE ISMH2-10C30CD) with an incremental encoder (INOVANCE EI34H) are combined into the main circuit of the setup. A DSP (TMS320F2812PGFA) and a CPLD (EPM240T100I5N) are selected as the control circuit.

The main parameters of the PMSM and the proportional controller in the experiment are same as the simulation parameters in Tab. I. The maximal threshold of the repetitive number P_M in (9) is selected as 3 to prevent overrun due to the calculating and storage limitations of the platform.

A sinusoidal wave with 4rad amplitude, 0.5Hz and zero initial phases is used as the reference signal in the experiment. The reference and rotor position experimental waveforms are shown in Fig. 15. As shown in the figures, the actual rotor position signal had been tracking the reference successfully with delay time about 50 ms.

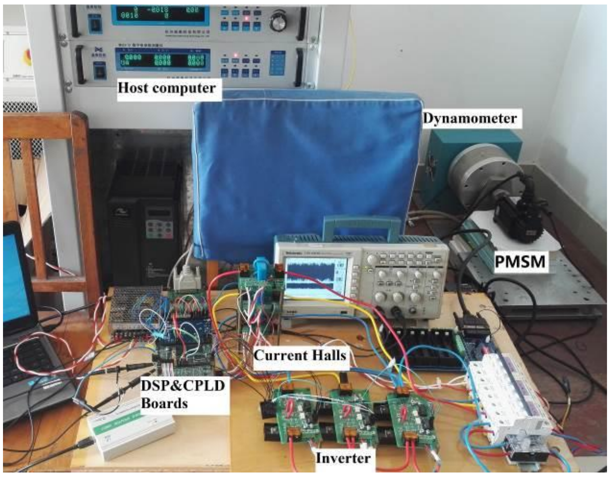

Fig. 14. Experimental platform.

A rated load torque T_L is uploaded on the shaft when the system is operating in the steady state. The experimental waveforms of θ^*, θ, ω_r and T_L are shown in Fig. 16. The figure shows that the rotor position is almost not influenced when the load torque is uploaded.

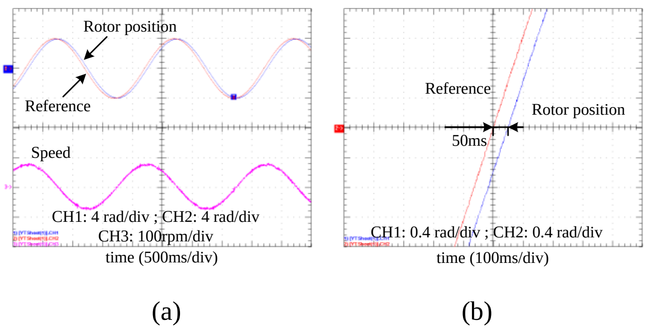

Fig. 15. Experimental waveforms for the proposed method. (a) Rotor position and speed waves, (b)Part enlarged rotor position waves.

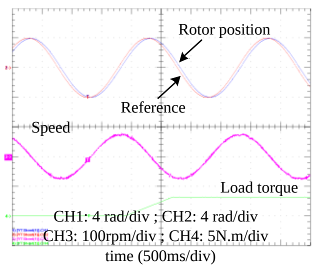

Fig. 16. Experimental waveforms for the proposed method with rated load torque.

The experimental results of the proposed method with stator resistance mismatches of R_{se}/R_s = 0.0001 and 850 are shown in Fig. 17. The figures show that the system with negative mismatches of the proposed method can be controlled stably. For positive mismatch of 850, the control objectives can be satisfied, and the operating performance become worse when the positive mismatch exceeds 850.

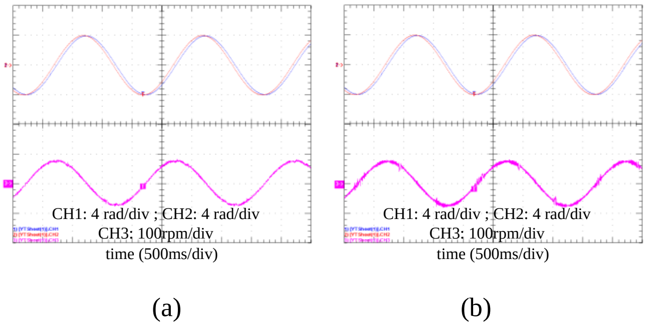

Fig. 17. Experimental waveforms for the proposed method with stator resistance mismatch. (a) Positive mismatch, (b) Negative mismatch.

Similarly, according to the experimental results of the stator induction and magnet flux linkage mismatches for the proposed method, they can be stably controlled within L_{se}/L_s = 0.1~125 and ψ_{me}/ψ_m = 0.2~8. Comparing with the simulation results, the stable ranges of the experimental results are somewhat reduced, this is caused by noises and hardware parameter variations during the operating process.

Experimental waveforms of the improved NMPSC with the repetitive number equalling to 3, i. e. the variable N_p is selected as 2 in (Younesi et al., Jan. 2018) and (Younesi et al. Nov. 2018), are shown in Fig. 18. As shown in the figure, the speed waveform is distorted obviously, and the delay time is almost the same as the proposed method. Comparing with the improved method with rotor position ITAE as 2.734, the ITAE of the proposed method is 2.682 during four cycles of the sinusoidal reference. Moreover, the control performance can be further improved if the processor can be further improved with more predictive processes in a sampling period.

6. CONCLUSIONS

In this paper, a NMPSC with variable predictive horizon is proposed to be applied to the PMSM rotor position control system. The proposed method provides a suitable predictive horizon in each sampling period with fewer calculation burden and better performance. Comparing with the improved NMPSC strategy, the performances of the proposed method are analysed and verified by simulation and experimental results under the same conditions.

The servo stiffness of the system with NMPSC with variable predictive horizon is increased at least about 9.898%, and the robustness of the stator resistance and magnet flux linkage are improved about 85.0% and 54.77% respectively according to the simulation results.

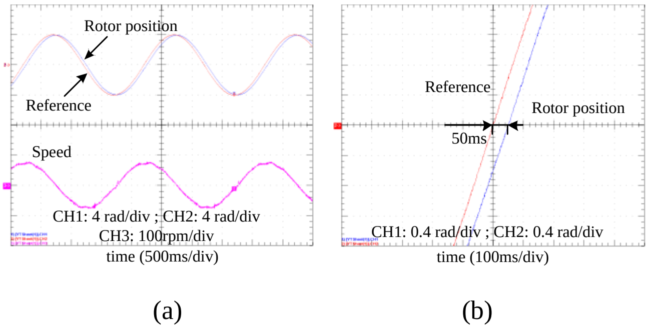

Fig. 18. Experimental waveforms for the improved NMPSC method. (a) Rotor position and speed waves, (b)Part enlarged rotor position waves.

The experimental rotor position ITAE for the proposed method is decreased about 1.902% comparing with the improved NMPSC. Due to the limitation of experimental platform, the maximal threshold P_M is restricted to a small value. If the system can operate at a larger P_M, the control performance can be further improved, because more predictive processes can be calculated in a single sampling period to further extend the predictive horizon.

REFERENCES

A. Younesi, S. Tohidi, and M. R. Feyzi (2018). Improved Optimization Process for Nonlinear Model Predictive Control of PMSM. *Iranian J. Elect. & Electron. Eng.*, 14(3), 278 - 288.

A. Younesi, S. Tohidi, M. R. Feyzi, et al. (2018). An improved nonlinear model predictive direct speed control of permanent magnet synchronous motors. *International Trans. Elect. Energy Syst.*, 16, 2535 - 2550.

B. Kou and S. Cheng. *AC Servo Motor and Control*, 1st ed. Beijing, China: China Machine Press, 2008.

D. Tavernini, M. Metzler, P. Gruber, et al. (2019). Explicit Nonlinear Model Predictive Control for Electric Vehicle Traction Control. *IEEE Trans. Control Syst. Technol.*, 27(4), 1438 - 1451.

F. Wang, H. Xie, Q. Chen, et al. (2020). Parallel Predictive Torque Control for Induction Machines Without Weighting Factors. *IEEE Trans. Power Electron.*, 35(2), 1779 - 1788.

F. Wang. *Control System Analysis and Design – Process Control System*. 1st ed. Beijing, China: Tsinghua University Press, 2014.

H. Guo, F. Liu, F. Xu, et al. (2019). Nonlinear Model Predictive Lateral Stability Control of Active Chassis for Intelligent Vehicles and Its FPGA Implementation. *IEEE Trans. Syst., Man, Cybern., Syst.*, 49(1), 2-13.

H. T. Nguyen and J. Jung (2018). Asymptotic Stability Constraints for Direct Horizon-One Model Predictive Control of SPMSM Drives. *IEEE Trans. Power Electron.*, 33(10), 8213 - 8219.

H. Xiao and C. L. P. Chen (2019). Incremental Updating Multirobot Formation Using Nonlinear Model Predictive Control Method With General Projection Neural Network. *IEEE Trans. Ind. Electron.*, 66(6), 4502-4512.

J. Rodriguez and P. Cortes (2012). *Predictive Control of Power Converters and Electrical Drives*. 1st ed. Chichedter, U.K.: IEEE Press-Wiley.

L. Dong, J. Yan, X. Yuan, et al. (2019). Functional Nonlinear Model Predictive Control Based on Adaptive Dynamic Programming. *IEEE Trans. Cybern.*, 49(12), 4206-4218.

L. Yan, F. Wang, M. Dou, et al. (2020). Active Disturbance-Rejection-Based Speed Control in Model Predictive Control for Induction Machines. *IEEE Trans. Ind. Electron.*, 67(4), 2574-2584.

M. Andrés, C. D. Roberto, P. A. Ricardo, et al. (2019). Computationally Efficient Cascaded Optimal Switching Sequence MPC for Grid-Connected Three-Level NPC Converters. *IEEE Trans. Power Electron.*, 34(12), 12464 - 12475.

M. Norambuena, J. Rodriguez, Z. Zhang, et al. (2019). A Very Simple Strategy for High-Quality Performance of AC Machines Using Model Predictive Control. *IEEE Trans. Power Electron.*, 34(1), 794 - 800.

M. S. Mubarok and T. Liu (2019). Implementation of Predictive Controllers for Matrix-Converter-Based Interior Permanent Magnet Synchronous Motor Position Control Systems. *IEEE J. Emerg. Sel. Topics Power Electron.*, 7(1), 261-273.

M. Siami, D. A. Khaburi and J. Rodriguez (2017). Torque Ripple Reduction of Predictive Torque Control for PMSM Drives with Parameter Mismatch. *IEEE Trans. Power Electron.*, 32(9), 7160-7168.

N. Vafamand, M. M. Arefi, M. H. Khooban, et al. (2019). Nonlinear Model Predictive Speed Control of Electric Vehicles Represented by Linear Parameter Varying Models With Bias Terms. *IEEE J. Emerg. Sel. Topics Power Electron.*, 7(3), 2081-2089.

P. Cortes, J. Rodriguez, C. Silva, et al. (2012). Delay Compensation in Model Predictive Current Control of a Three-Phase Inverter. *IEEE Trans. Ind. Electron.*, 59(2), 1323-1325.

T. Geyer. *Model predictive control of high power converters and industrial drives*, 1st ed. Chichedter, U.K.: Wiley, 2016.

W. Wu, D. Wang and L. Liu (2019). A Multi-Layer Sequential Model Predictive Control of Three-Phase Two-Leg Seven-Level T-Type Nested Neutral Point Clamped Converter Without Weighting Factors. *IEEE Access*, 7, 162735-162746.

X. Gao, M. Abdelrahem, C. M. Hackl, et al. (2020). Direct Predictive Speed Control With a Sliding Manifold Term for PMSM Drives. *IEEE J. Emerg. Sel. Topics Power Electron.*, 8(2), 1258-1267.

X. Wang and D. Sun (2017). Three-Vector-Based Low-Complexity Model Predictive Direct Power Control Strategy for Doubly Fed Induction Generators. *IEEE Trans. Power Electron.*, 32(1), 773 - 782.

Y. Chen, N. Scarabottolo, M. Bruschetta, et al. (2020). Efficient move blocking strategy for multiple shooting-based non-linear model predictive control. *IET Control Theory & Applications*, 14(2), 343-351.

Y. E. G. Vera, R. Dufo-López and J. L. Bernal-Agustin (2019). Energy Management in Microgrids with Renewable Energy Sources: A Literature Review. *Applied Sciences*, 9(18), 3854-3882.

Y. Wei, Y. Wei, Y. Sun, et al. (2020). Prediction Horizons Optimized Nonlinear Predictive Control for PMSM Position System. *IEEE Trans. Ind. Electron.*, 67(11), 9153 - 9163.

Y. Zhang and H. Yang (2016). Two-Vector-based Model Predictive Torque Control Without Weighting Factors for Induction Motor Drives. *IEEE Trans. Power Electron.*, 31(2), 1381-1390.

Y. Zhang, J. Jin and L. Huang (2020). Model-Free Predictive Current Control of PMSM Drives Based on Extended State Observer Using Ultra-Local Model. *IEEE Trans. Ind. Electron.(Early Access)*.

Z. Sun, L. Dai, K. Liu, et al. (2019). Robust Self-Triggered MPC With Adaptive Prediction Horizon for Perturbed Nonlinear Systems. *IEEE Trans. Autom. Control*, 64(11), 4780-4787.

Z. Wang, A. Yu, X. Li, et al. (2019). A Novel Current Predictive Control Based on Fuzzy Algorithm for PMSM. *IEEE J. Emerg. Sel. Topics Power Electron.*, 7(2), 990-1001.

Z. Zhang, C. M. Hackl, and R. Kennel (2017). Computationally Efficient DMPC for Three-Level NPC Back-to-Back Converters in Wind Turbine Systems With PMSG. *IEEE Trans. Power Electron.*, 32(10), 8018 - 8034.